ICMIEE22-071

Numerical Analysis of the Aerodynamic Characteristics of NACA 2413 Airfoil

Md Ramijul Alam[1*], *Arnob Dey*[2], *Md. Golam Kader*[3]
[1,2,3] Department of Mechanical Engineering, Khulna University of Engineering & Technology, Khulna-9203, BANGLADESH

ABSTRACT

The current investigation primarily focuses on the variability of the aerodynamic characteristics of the NACA-2413 airfoil for different turbulent models (Realizable k-ε Model, Standard k-ε Model, and Shear-Stress Transport (SST) k-ω Model) in different Reynolds Numbers. The aerodynamic characteristics such as lift force, drag force, lift-to-drag ratio, and pressure distribution were evaluated at several angles of attack for different Reynolds numbers (Re = 7×10^5, 3×10^6, and 6×10^6) using Ansys Fluent 2020R2. The numerical results indicate that the lift coefficient increased with the angle of attack up to the stalling point. Though the different turbulent models exhibited nearly the same value at a lower angle of attack, however, produced different values for the higher angles of attack (at $\alpha = 10^{\circ}$ for Re = 3×10^6), which is also visible in the velocity and pressure contours. Again, at the lower Reynolds number, the different turbulent model shows considerably different value but this difference is reduced with the increase in Reynolds number. For all the conditions, the k-ε model produces a higher lift value in comparison to the SST k-ω model. However, in the SST k-ω model, separation occurs at a smaller angle of attack as compared to the other two models, because the SST k-ω model more accurately resolves the viscous layer and flow separation for high-pressure gradients than the other two models. Furthermore, with the increase in Reynolds number, the deviation between these three turbulent models decreases significantly. At high Reynolds numbers, the realizable k- ε model and the standard k- ε model produce nearly identical results.

Keywords: Airfoil; SST k- ω Model; k- ε Model; Lift Coefficient; Drag Coefficient

1. Introduction

The study of an airfoil holds great importance in aerodynamics as the efficacy of the aerodynamic body largely depends on the shape and aerodynamic properties of an airfoil. An airfoil is the cross-section of a body that is positioned in an airstream to produce effective aerodynamic force. The cross-section of wings, propeller blades, windmill blades, compressor, turbine blades in a jet engine, and hydrofoils are popular examples of airfoils [1]. The influence of pressure and shearing stress distribution over the surface causes aerodynamic forces and moments on an aerodynamic body [2]. When the air flows over an aerodynamic body, two perpendicular forces are generated: one is normal to the flow direction, called the lift force, and another is parallel to the flow direction, called the drag force [2]. The lift force can be generated if the fluid comprises circulation around a body, like the flow around a spinning cylinder. However, the key concern in the study of an airfoil is to increase the lift force and reduce the drag force optimally. Though the lift is high and the drag is low at small angles of attack, the lift drops precipitously and the drag increases as the angles of attack (α) increase after a certain point known as the stalling point. As a result, the angle of attack at the stalling point and the lift (L) to drag (D) ratio for a given velocity play a crucial role in aerodynamics [2]. However, at a particular angle of attack, the lift (L) to drag (D) ratio increases with the free stream velocity up to a certain point, then decreases again with augmented velocity [2]. The aerodynamic properties of an airfoil can be determined experimentally by placing an airfoil in a wind tunnel and monitoring the velocity and pressure distribution across its surface. Identically, these experiments can also be done utilizing a Computational Fluid Dynamics (CFD) approach [3].

The NACA (which stands for National Advisory Committee for Aeronautics, NASA's precursor) database is the primary source of airfoil models which has a large number of airfoil models that can be utilized for CFD modeling [4]. Sarkar et al. [5] numerically evaluated the pressure distribution, velocity distribution, various aerodynamic forces, lift to drag ratio, stall region, and the critical angle of attack over the NACA 2412 airfoil model at a high Reynolds number of $7.6659*10^6$ through the Shear Stress Transport Turbulent Model. Mehdi et al. [6] numerically predicted aerodynamic characteristics at various Reynolds numbers and angles of attack and found that the coefficient of drag increases as the Reynolds number increases, owing to the enormous area beneath the airfoil yielding increased pressure drag and the growing separation zone on the upper surface of the airfoil. Sumaryada et al. [3] analyzed the performance of the NACA 4312 airfoil at various arriving airspeeds and gurney flap angles, concluding that increasing the gurney flap angles to 45 and 90 would increase the airfoil's lifting force while lowering the drag force. For totally laminar and totally turbulent flow regimes, Asraf et al. [7] quantitatively modeled the effect of altering airfoil thickness and chamber on plunging and combined pitching and plunging airfoil propulsion at different Reynolds numbers. The thickness study involved 2-D NACA symmetric airfoils with 6–50 percent thick

* Corresponding author. Tel.: +88-01751746432
E-mail addresses: ramij.kuetme16@gmail.com

sections that were subjected to pure plunging motion at reduced frequency k=2 and amplitudes h=0.25 and 0.5, as well as combined pitching and plunging motion at k=2, h=0.5, phase=90°, pitch angle o=15° and 30°, and the pitch axis was located at 1/3 of the chord from the leading edge. Hasan et al. [9] investigated the NACA 0018 model between Reynold's number 300,000 and 600,000 for different angles of attack. When comparing the results of other simulation models, the SST k-ω model produces the most accurate findings.

There are a large number of literatures concerning the numerical investigation of aerodynamic characteristics of NACA airfoil, yet a little clarity on the aerodynamic properties of NACA-2413 airfoil. Additionally, aerodynamic properties of NACA-2413 airfoil for the different turbulent model's output for different Reynolds numbers are not clear in the literature. Furthermore, the variation of the results due to the change of the Reynolds number are not clear for these three turbulent models. Hence, the current study employs a numerical investigation to predict the aerodynamic characteristics of the NACA 2413 airfoil at various angles of attack and Reynolds numbers for three different turbulent models (Realizable k-ε Model, Standard k-ε Model, and Shear-Stress Transport (SST) k-ω Model) and compare the results to find the deviations of these results with the change of the Reynolds number.

2. Computational Method

The numerical simulation begins with the generation of the chosen airfoil geometry (NACA 2413), shown in **Fig.1** in an online airfoil generator [4], and the coordinates are then imported to generate the geometry of the airfoil. The obtained coordinates were then imported to SOLIDWORK 2018 to create the desired geometry, and then this geometry was imported to the ANSYS design module. The current investigation uses ANSYS 2020 R2 software for numerically evaluating the results. From the airfoil nomenclature of the NACA 2413 asymmetrical airfoil, the maximum chamber is 0.02c, located at 0.4c from the leading edge, and the maximum thickness is 0.13c, where, c denotes the chord length [2]. The three turbulence models (Realizable k-ε Model, Standard k-ε Model, and Shear-Stress Transport (SST) k-ω Model) were used to solve the problem in a steady state with fixed Reynolds number (Re = 7×10^5, 3×10^6, and 6×10^6). Air is used as the fluid media, and its density (ρ) and viscosity (μ) are assumed as constant, where ρ = 1.225 kg/m^3 and μ = $1.7894*10^{-5}$ kg/ms [11]. The least-square cell-based gradient option was used to solve the steady-state Reynolds Average Navier-Stokes (RANS) equation, and the coupled pressure-based solver was used with the second-order scheme for enhanced accuracy. The steady-state RANS equations can be expressed as:

$$\frac{\partial}{\partial x_i}(\rho u_i) = 0 \quad (1)$$

$$\frac{\partial}{\partial x_j}(\rho u_i u_j) = -\frac{\partial}{\partial x_i}(p) + \frac{\partial}{\partial x_j}\left[\mu\left(\frac{\partial u_i}{\partial x_j} + \frac{\partial u_j}{\partial x_i} - \frac{2}{3}\delta_{ij}\frac{\partial u_l}{\partial x_l}\right)\right] + \frac{\partial}{\partial x_j}(-\rho\overline{u_i' u_j'}) \quad (2)$$

Additional terms appear in the equation represent the effects of turbulence. This Reynolds stresses $-\rho\overline{u_i' u_j'}$ must be modeled to solve the RANS equation. This nonlinear term in RANS equation can be solved by different turbulence models. In order to predict the effects of turbulence in the flow over the airfoil, the standard k-ε Model, the Realizable k- ε model, and the SST k-ω model is used in this investigation.

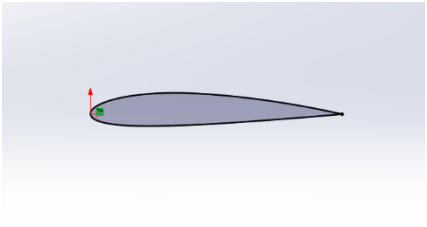

Fig.1 2D view of NACA 2413 airfoil.

2.1 Standard k-ε Model

The k-epsilon turbulence model is two equation method, used in Computational Fluid Dynamics (CFD), and it allows to obtain both a turbulent length and time scale by solving two different transport equations [12]. Due to its resilience, economy, and realistic accuracy for a wide variety of turbulent flows have made it useful in industrial flow and heat transfer simulation. The standard k-ε Model is a model based on model transport equations for the turbulence kinetic energy (k) and its dissipation rate (ε)[13].

The turbulence kinetic energy k and its rate of dissipation ε are obtained from the following transport equations:

$$\frac{\partial}{\partial x_i}(\rho k u_i) = \frac{\partial}{\partial x_j}\left[\left(\mu + {}^{\mu_t}/_{\sigma_k}\right)\frac{\partial k}{\partial x_j}\right] + G_k + G_b - \rho\varepsilon - Y_M + S_K \quad (3)$$

$$\frac{\partial}{\partial x_i}(\rho\varepsilon u_i) = \frac{\partial}{\partial x_j}\left[\left(\mu + {}^{\mu_t}/_{\sigma_\epsilon}\right)\frac{\partial \varepsilon}{\partial x_j}\right] + C_{1\varepsilon}\frac{\varepsilon}{k}(G_k + C_{3\varepsilon}G_b℃) - C_{2\varepsilon}\rho\frac{\varepsilon^2}{k} + S_\varepsilon \quad (4)$$

In these equations, G_k, Y_M, G_b,$C_{1\varepsilon}$, C_2,$C_{3\varepsilon}$, σ_k , σ_ϵ,S_K, S_ε are the turbulence kinetic energy generation, the fluctuation in compressible turbulence to overall dissipation rate, turbulence kinetic energy generation constant, the turbulent Prandtl numbers for k and ε, user-defined source terms, respectively. However, μ_t is turbulent viscosity which is computed by combining k and ε and $\mu_t = \rho C_\mu {}^{k^2}/_{\varepsilon}$, where C_μ is a constant.

2.2 Realizable k-ε Model:

The realizable k-ε Model is different from the standard k-ε Model in two ways: it has an alternative formulation for turbulent viscosity and a modified transport equation for the dissipation rate ε, which is derived from a precise equation for the transport of mean-square vorticity fluctuation. Shih et al. [14] proposed the Realizable k-ε Model to address limitations of traditional k-ε models by introducing the following: a new eddy-viscosity formula involving a variable C_μ, first proposed

by Reynolds, and a new model equation for Dissipation (ε) based on the dynamic equation of the mean-square vorticity fluctuation. Because it includes the effects of mean rotation in the explanation of turbulent viscosity, the realizable k- ε model yields non-physical turbulent viscosity in circumstances when the computational domain contains both stationary and rotating fluid zones [13].

The modeled transport equations for k and ε in the realizable k-ε Model are:

$$\frac{\partial}{\partial x_j}(\rho k u_j) = \frac{\partial}{\partial x_j}\left[\left(\mu + {}^{\mu_t}/_{\sigma_k}\right)\frac{\partial k}{\partial x_j}\right] + G_k + G_b - \rho\varepsilon - Y_M + S_k \quad (5)$$

$$\frac{\partial}{\partial x_j}(\rho\varepsilon u_j) = \frac{\partial}{\partial x_j}\left[\left(\mu + {}^{\mu_t}/_{\sigma_\varepsilon}\right)\frac{\partial \varepsilon}{\partial x_j}\right] + \rho C_1 S\varepsilon - \rho C_2 \frac{\varepsilon^2}{k+\sqrt{v\varepsilon}} + C_{1\varepsilon}\frac{\varepsilon}{k}C_{3\varepsilon}G_b + S_\varepsilon \quad (6)$$

where $C_1 = \max\left[0.43, \frac{\eta}{\eta+5}\right]$, $\eta = S\,{}^{k}/_{\varepsilon}$, $S = \sqrt{2S_{ij}S_{ij}}$

In these equations, G_k, Y_M, G_b,$C_{1\varepsilon}$, C_2,$C_{3\varepsilon}$, σ_k , σ_ϵ,S_K, S_ε are the turbulence kinetic energy generation, the fluctuation in compressible turbulence to overall dissipation rate, turbulence kinetic energy generation constant, the turbulent Prandtl numbers for k and ε, user-defined source terms, respectively.

2.3 Shear-Stress Transport (SST) k-ω Model:

In order to achieve the stable and precise formulation of the k-ω model in the near-wall region with the free stream independence of the k-ε model in the far-field region, the k-ε Model is turned into a k-ω formulation [15]. The two equations of SST k-ω turbulence model provides a general solution for the specific dissipation rate of turbulent viscosity (ω) and the turbulent kinetic energy (k) [13]. The SST k-ω Model is more stable and accurate than the standard k-ω model for a vast range of flow like adverse pressure gradient flow, airfoils, and transonic shock waves. The transport equations of the SST k-ω model is:

$$\frac{\partial}{\partial x_i}(\rho k u_i) = \frac{\partial}{\partial x_j}[(\mu + \sigma_k\mu_t)\frac{\partial k}{\partial x_j}] + G_k - Y_k + S_k \quad (7)$$

$$\frac{\partial}{\partial x_j}(\rho\omega u_j) = \frac{\partial}{\partial x_j}[(\mu + \sigma_\omega\mu_t)\frac{\partial \omega}{\partial x_j}] + G_\omega - Y_\omega + D_\omega + S_\omega \quad (8)$$

in these equations, G_k, G_ω,Y_ω , Y_k,σ_k, σ_ω,D_ω,S_k, S_ω are the turbulent kinetic energy generation is due to the mean velocity gradient, generation of ω, dissipation of k, dissipation of ω, turbulent Prandtl number for k and ω, the cross-diffusion term, user-defined source terms, respectively. The turbulent viscosity is computed by:

$$\mu_t = \frac{\rho k}{\omega}\frac{1}{\max\left[\frac{1}{\alpha^*}, \frac{SF_2}{a_1\omega}\right]} \quad (9)$$

3. Boundary Condition

A computational domain was created around the NACA 2413 airfoil for doing the simulation. First of all, the chord length of the NACA 2413 airfoil was taken to be equal to 1000mm. From the trailing edge, the domain was expanded 12.5c upstream and 20c downstream, showed in **Fig. 2**. EABCD was assumed to the constant velocity inlet, and DE was assumed as the pressure outlet, showed in **Fig. 2**. But the airfoil surface was considered to be the no-slip condition. The angle of attack was entered into the fluid by changing the entering flow direction and dividing it into components rather than rotating the airfoil. This velocity component didn't affect the final results. The x velocity component was taken as u cos α and y velocity component was $u \sin \alpha$.

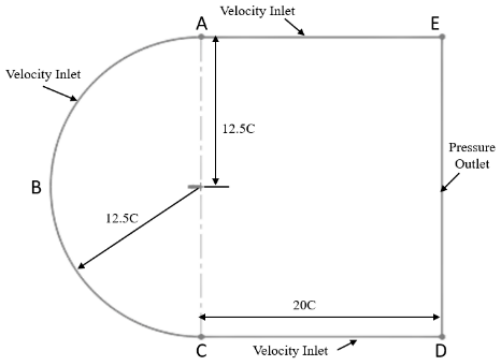

Fig.2 Computational domain with boundary conditions.

3.1 Grid Generation and Independency Test

The grid generation is an essential part of simulation. The C-type grid topology is created for better near-wall mesh quality and also to have convenient convergence properties. ANSYS Meshing is used to create a C-type structural mesh with quadrilateral elements, showed in **Fig. 3**. For the current simulation, the value of y^+ was higher than 30 and lowered then 50.

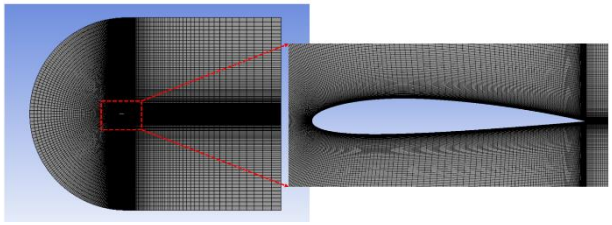

Fig.3 Structural mesh of the domain.

In order to get the optimized mesh size, a set of numerical simulations was conducted for multiple numbers of mesh by altering the edge sizing of circular and rectangular parts.

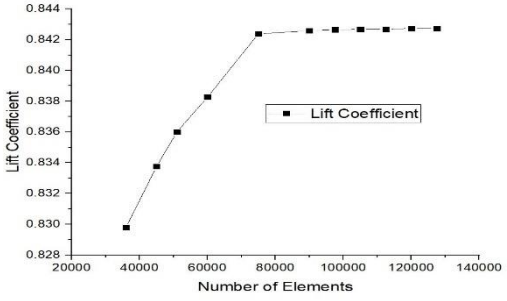

Fig.4 Variation of lift with the number of elements.

After comparing the result, the best mesh was determined. From the **Fig. 4**, the mesh size higher than 90000 number of elements does not show much variations in lift coefficient and hence chosen for the current simulation.

3.2 Validation

For the model validation, the numerical data of NACA 2412 is validated with experimental value (NASA-CR-197497) [16] at Reynold's number 2.2×10^6 and Mach number 0.13 at different angle of attack. In addition, numerical data of NACA 0012 is compared with experimental value by Ladson, 1988 [17] at Reynold's number 6×10^6 and Mach number 0.15 at different angle of attack. The SST k-ω model is used for the validation. From the graph in **Fig. 5**, it is observed that both the experimental value and numerical value are almost similar. So, the numerical simulation of NACA 2413 airfoil is conducted using similar set up.

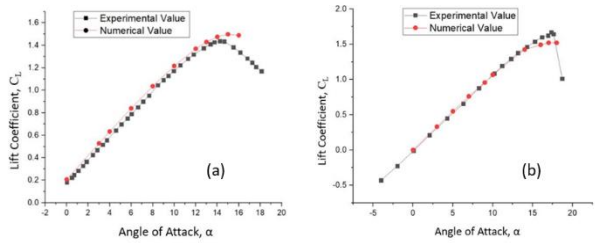

Fig.5 Lift coefficient vs angle of attack for Experimental and Numerical value of (a) NACA 2412 (b) NACA 0012

4. Result and Discussion

The variation of lift coefficient with the changes in the angle of attacks are depicted in **Fig. 6**, for three turbulent models, and it is observed that lift increased linearly with the angles of attack up to a certain value.

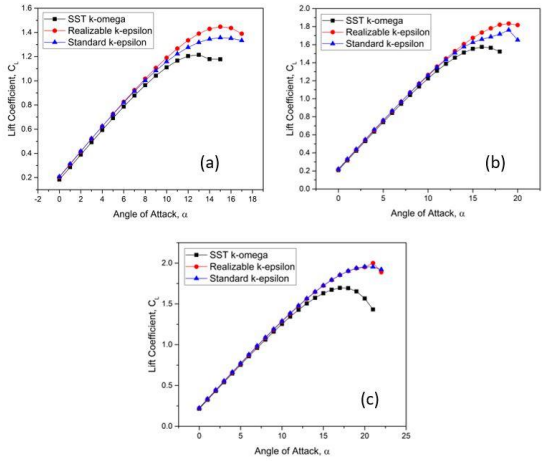

Fig.6 Lift coefficient vs. Angle of attack at Reynold's number (a)7×10^5, (b)3×10^6, and (c)6×10^6.

Furthermore, the lift coefficient increases with the increase in Reynolds number, and then decreased with the increased angle of attack because of the flow separation. Again, in the SST k-ω model, separation occur at a small angle of attack at $\alpha = 13^{\circ}$, but in Realizable k-ε and Standard k-ε model, it occurs at $\alpha = 15^{\circ}$ with higher lift coefficient. This is because the SST k-ω model resolves the viscous layer and also the flow separation with a high-pressure gradient more accurately as compared to the other model. The Realizable k-ε and Standard k-ε model produces almost the same lift coefficient up to $\alpha = 7^{\circ}$ at Re= 7×10^5, $\alpha = 11^{\circ}$ at Re= 3×10^6 and $\alpha = 19^{\circ}$ at Re= 6×10^6. So, as the Reynolds number increases, the Realizable k-ε and Standard k-ε model produce similar lift coefficient value at higher angle of attacks. Moreover, for all the conditions, the k-ε model produces a higher lift value in comparison to the SST k-ω model. The k-ε models predict stall at a higher angle of attack as compared to the SST k-ω model for all the three Reynolds number conditions which is depicted in **Fig. 6.**

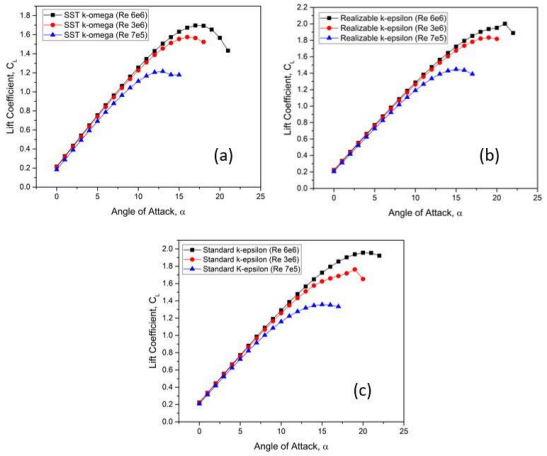

Fig.7 Lift coefficient vs. Angle of attack at three Reynold's number for (a) SST k-ω Model, (b) Realizable k-ε Model, and (c) Standard k-ε Model.

From **Fig. 7**, it can be observed that lift increase with the increase in Reynolds number for NACA 2413. The critical angle of attack also increases with an increase in Reynolds number. Critical angle of attack is defined as the angle of attack where the lift coefficient will be maximum, or the stalling occurs. Lift coefficient increase linearly up to the critical angle of attack and then decrease precipitously and this is happened due to the flow separation in the trailing edge. From **Fig. 7a**, at Reynold's number 7×10^5, the critical angle of attack lies between 12° and 13°. But the critical angle of attack increases with the increase in Reynold's number, up to 17° for Reynold's number 6×6^6. Similarly**, Fig. 7b** and c shows that the lift coefficient increases with the increase in Reynold's number in Realizable and Standard k- ε Turbulent model. In **Fig. 7b**, the critical angle of attack lies between 14° and 15° for Reynold's number 7×10^5, which is higher than the value found in **Fig.7a** at the same

Reynold's number. At Reynold's number 6×10^6, the critical angle of attack was found in between 20° to 21°. Again, in **Fig. 7c**, the critical angle of attack lies between 14° and 15° for Reynold's number 7×10^5, similar for Realizable k- ε Turbulent model at the same Reynold's number. At Reynold's number 6×10^6, the critical angle of attack was found in between 20° to 21°. **Fig. 7** also shows the same type of results at a higher Reynold's number.

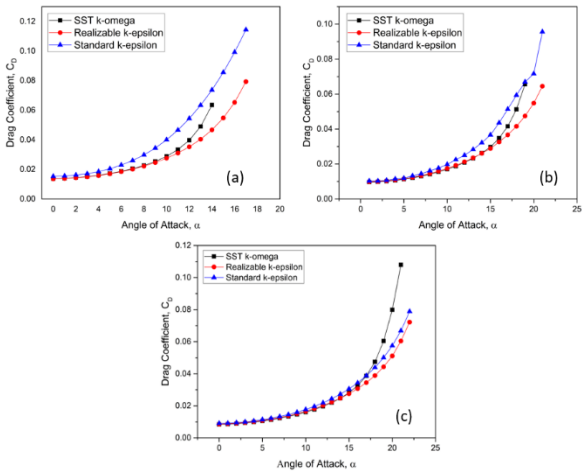

Fig.8 Drag coefficient vs. Angle of attack at Reynold's number (a)7×10^5, (b)3×10^6, and (c)6×10^6.

Fig. 8 depicts the change in the drag coefficient with the change in angle of attack. Here, for c, the drag coefficient is increased with the angle of attack and almost the same up to an angle of attack 8° for the above three turbulent models. However, after the angle of attack 15°, the drag coefficient increases sharply for the SST k-ω model compared to the k-ε model, shown in **Fig. 8c**. The standard k-ε model produces higher drag in comparison to other two model. **Fig. 8a** and **b** also illustrate the same kind of output, however, considering the **Fig. 8** a, b, and c, it can be observed that the Standard k-ε model produces a higher drag coefficient in comparison to the Realizable k-ε model and the SST k-ω model, but this difference decreases as the increase in Reynold's number. After the flow separation, the drag coefficient increases with the further increase in the angle of attack, in contrast, to decrease in lift coefficient.

4.1 Pressure and Velocity contour

Fig. 9 and **Fig. 10**, represents the pressure and velocity contours only for the SST k- ω model at Reynold's number 6×10^6 at a different angle of attack. The contours are almost similar for a fixed Reynold number at a low angle of attack, however, as the angle of attack increases, the contour varies for the different turbulent models. Again, it is clearly observed that there is higher pressure at the lower surface and lower pressure at the higher surface of the airfoil. It is also observed that there is a negative pressure along the whole upper surface of the airfoil. As the angle of attack increases the pressure on the lower surface increases, but the pressure on the upper surface reduces further with the angle of attack. Due to this pressure distribution, the lift is generated on the airfoil. The pressure difference between the lower and upper surface increases with the angle of attack until the stall or flow separation on the upper surface occurs. Again, at a fixed Reynold's number and lower angle of attack, the pressure difference between the upper and lower surfaces is almost the same for all these three turbulent models, however, these three models show different result from each other as the angle of attack become high.

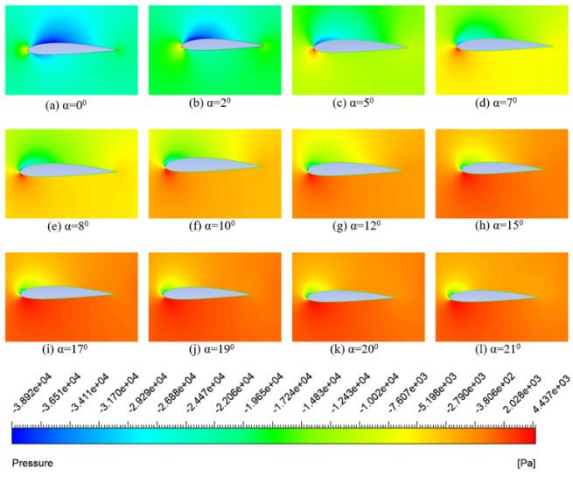

Fig.9 Pressure contours for different angle of attack for SST k- ω model at Reynold's number 6×10^6.

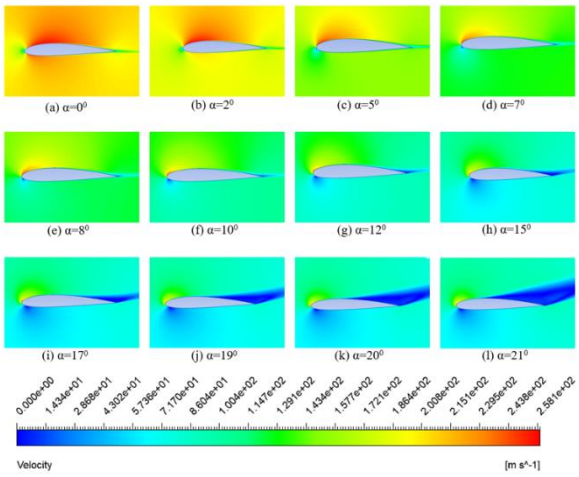

Fig.10 Velocity contours for different angle of attack for SST k- ω model at Reynold's number 6×10^6.

In the Realizable k- ε model and Standard k- ε model, there is an almost similar pressure difference. But in the SST k- ω model, there is a pressure difference lower than the other two models. Again, at lower Reynold's number, the pressure difference is significant between these three models, but with the increase in Reynold's number,

pressure difference reduces for these models. For all the cases, the Realizable k- ε model gives higher pressure difference, and the SST k- ω model gives a lower pressure difference between the upper and lower surface. This variation of velocity contour can observe by velocity magnitude but the pattern remains almost similar. Again, it is clearly observed that there is a higher velocity at the upper surface and lower velocity at the lower surface of the airfoil. It is observed that at the lower angle of attack the flow is attached to the surface of the airfoil but at the higher angle of attack, flow separation starts to occur at the trailing edge. As the angle of attack increases further, this flow separation starts to move toward the leading edge which can also observe from the velocity contour. Due to this flow separation at such a higher angle of attack, the lift coefficient also decreases after this angle of attack. In SST k- ω model, the flow separation occurs at lower angle of attack compare to the Realizable k- ε model and Standard k- ε model for all the three fixed Reynold's number.

5. Conclusion

The current study investigates the aerodynamic characteristics of the 2D NACA 2413 airfoil at different angle of attack and at different Reynolds number 7×10^5, $3\times10^{6,}$ and 6×10^6 with different turbulent models such as the Realizable k- ε model, Standard k- ε model, and SST k- ω model. In this investigation, it is clearly observed that at higher Reynolds number these three models produce almost similar results. As the angle of attack increases the lift coefficient increases almost similarly in these three turbulent models. The difference of the magnitude is very small at the lower angle of attack but at the higher angle of attack, the magnitude varies significantly. But at all the angles of attack, the nature of the graph is similar. Moreover, flow separation occurs at a different angle of attack for different turbulent models. In SST k-ω model, the flow separation occurs at lower angle of attack compare to the Realizable k-ε model and Standard k-ε model for all the three fixed Reynold's number. As the SST k-ω model resolves the viscous layer and also the flow separation with a high-pressure gradient more accurately as compared to the other model, SST k-ω model is found to be the best suit for the current analysis.

6. References

[1] Kevadiya, M., & Vaidya, H. A. (2013). 2D analysis of NACA 4412 airfoil. *International Journal of Innovative Research in Science, Engineering and Technology*, *2*(5), 1686-1691.

[2] Anderson Jr, J. D. (2010). *Fundamentals of aerodynamics*. Tata McGraw-Hill Education.

[3] Sumaryada, T., Jaya, A. M., & Kartono, A. (2018). Simulating the Aerodynamics Profiles of NACA 4312 Airfoil in Various Incoming Airspeed and Gurney Flap Angle. *Omega: Jurnal Fisika dan Pendidikan Fisika*, *4*(1), 1-1.

[4] http://airfoiltools.com/airfoil/naca4digit

[5] Sarkar, S., & Mughal, S. (2017). CFD Analysis of Effect of Flow over NACA 2412 Airfoil through the Shear stress Transport Turbulence Model. *Int J Mech Pro Eng*, *5*(7), 58-62.

[6] Mehdi, H., Gaurav, S., & Sharma, M. (2016). Numerical investigation of fluid flow and aerodynamic performance on a 2D NACA-4412 airfoil. *International Journal of Research in Engineering and Innovation*, *1*(1), 1-5.

[7] Ashraf, M. A., Young, J., & Lai, J. C. S. (2011). Reynolds number, thickness and camber effects on flapping airfoil propulsion. *Journal of Fluids and structures*, *27*(2), 145-160.

[8] Cengel, Y. A., & Cimbala, J. M. (2017). Fluid mechanics: fundamentals and applications.

[9] Hassan, G. E., Hassan, A., & Youssef, M. E. (2014). Numerical investigation of medium range re number aerodynamics characteristics for NACA0018 airfoil. *CFD letters*, *6*(4), 175-187.

[10] Versteeg, H. K., & Malalasekera, W. (2007). *An introduction to computational fluid dynamics: the finite volume method*. Pearson education.

[11] Marshall, J., & Plumb, R. A. (1989). *Atmosphere, ocean and climate dynamics: an introductory text*. Academic Press.

[12] Launder, B. E., & Spalding, D. B. (1983). The numerical computation of turbulent flows. In *Numerical prediction of flow, heat transfer, turbulence and combustion* (pp. 96-116). Pergamon.

[13] Ansys Inc. (2013). Ansys fluent theory guide. *Canonsburg, PA, Release 15.0*.

[14] Shih, T. H., Liou, W. W., Shabbir, A., Yang, Z., & Zhu, J. (1995). A new k-ϵ eddy viscosity model for high reynolds number turbulent flows. *Computers & fluids*, *24*(3), 227-238.

[15] Menter, F. R. (1994). Two-equation eddy-viscosity turbulence models for engineering applications. *AIAA journal*, *32*(8), 1598-1605.

[16] Seetharam, H. C., & Rodgers, E. J. (1997). Experimental Studies of Flow Separation of the NACA 2412 Airfoil. *NASA CR*, *197497*.

[17] Ladson, C. L. (1988). *Effects of independent variation of Mach and Reynolds numbers on the low-speed aerodynamic characteristics of the NACA 0012 airfoil section* (Vol. 4074). National Aeronautics and Space Administration, Scientific and Technical Information Division.

NOMENCLATURE

α	: Angle of attack
C	: Chord length
C_D	: Coefficient of drag
C_L	: Coefficient of lift
ρ	: Density of the fluid
μ	: Kinematic viscosity
CFD	: Computational Fluid Dynamics
Re	: Reynolds Number
RANS	: Reynolds Averaged Navier-Stokes